Segregation at the $Pt_{0.5}Ni_{0.5}(111)$ surface studied by medium-energy ion scattering

S. Deckers, F. H. P. M. Habraken, and W. F. van der Weg
Department of Atomic and Interface Physics, University of Utrecht, P.O. Box 80000, 3508 TA Utrecht, The Netherlands

A. W. Denier van der Gon, B. Pluis, and J. F. van der Veen
FOM Institute for Atomic and Molecular Physics, Kruislaan 407, 1098 SJ Amsterdam, The Netherlands

R. Baudoing
Université Joseph Fourier, 38042 Grenoble, France

(Received 21 November 1989; revised manuscript received 6 April 1990)

Medium-energy ion scattering combined with shadowing and blocking is used to study the Pt-Ni alloy surface. By applying three scattering geometries in which different numbers of atomic layers are visible to the incoming ion beam, the compositions and relaxations of the first three layers of the crystal are accurately determined. An oscillating segregation profile is found in which (75±2)% Pt is present in the first layer, (27±3)% Pt in the second layer, and (53±5)% Pt in the third layer. The relaxations of the first and second interlayer distances amount to (−2.0±0.5)% and (−2.0±0.5)%. An enhancement of the thermal vibration amplitudes in the first three layers is found. The results support those obtained by other methods and agree with theoretical calculations.

I. INTRODUCTION

The investigation of alloy surfaces is both fundamentally interesting and chemically important. Theoretically, mechanisms of surface segregation and relaxation are not yet understood for many, particularly platinum-based, alloys. In heterogeneous catalysis there are many important reaction mechanisms which need a more profound understanding. Since nickel is able to crack saturated hydrocarbons, while platinum promotes the isomerization of these molecules, Pt-Ni alloys can be expected to give interesting variations in selectivity and reactivity for reactions involving organic molecules.

Chemisorptive and catalytic properties of Pt-Ni alloys have been investigated on small particles[1] and on polycrystalline and single-crystalline samples.[2,3] On single crystals it is found that alloying, for example, increases the activity for the hydrogenation of 1,3-butadiene, with a favorable increase in selectivity for the formation of butenes.[4] Also a difference in adsorption and desorption rates for H_2, C_6H_6, C_4H_4, and CO have been measured on Pt-Ni (111) surfaces.[5–7] These results called for an investigation of segregation effects in these alloys.

Surface segregation of Pt-Ni alloys has been studied for several compositions on two different crystal orientations: on $Pt_xNi_{1-x}(111)$ with $x=0.1$, 0.5, and 0.78 and on $Pt_xNi_{1-x}(110)$ with $x=0.1$ and 0.5. The analysis techniques used were low-energy electron diffraction using intensity-versus-voltage measurements (LEED *I-V*),[8–12] x-ray photoemission spectroscopy (XPS),[13,14] incidence-dependent excitation for Auger spectroscopy (IDEAS),[15] and low-energy ion scattering (LEIS).[16–18]

The results can be summarized as follows: for all studied systems, a large segregation effect is observed with oscillating platinum concentrations in the first three–four layers. On the close-packed (111) surface, the first layer is strongly enriched in platinum, the second layer in nickel, and the third layer slightly in platinum. In contrast, on the open (110) surface, the first layer contains almost exclusively Ni atoms, the second layer mostly Pt, the third layer again more Ni, and the fourth layer still a few percent more Pt atoms. The effects are less pronounced on the diluted alloys.

On the theoretical side, several general segregation studies have dealt with transition metal alloys. They all unambiguously predicted segregation of nickel, the element having the lowest surface free energy.[19–22] Recently, three more sophisticated approaches have been developed which have been used on the Pt-Ni system. These theories also take atom-size differences into account and use a new potential function. On the (111) surface the prediction of these theories does match the experiments reasonably well, but on the (110) surface the situation is more complicated. The embedded-atom model (EAM) (Ref. 23) predicts a metastable state in the 30–60 % Pt composition range, while the tight-binding Ising model (TBIM) gives a good prediction only for diluted alloys.[24,25] The thermodynamic Monte Carlo approach, which has been successfully applied to many alloy surfaces,[26–29] has recently been applied to Pt-Ni (Ref. 30) and has shown a reasonable agreement with LEED *I-V* measurements on both (111) and (110) surfaces.

Only a few techniques are suited for the investigation of segregation effects in more than one atom layer. LEED *I-V* combined with full dynamical calculations can give a three-layer resolution.[11] LEIS is only capable of measuring first-layer concentrations because of the large cross section for scattering and strong neutralization

effects.

Medium-energy ion scattering in combination with Shadowing and Blocking (MEIS-SB) has proven to be a valuable technique for measuring surface structures and relaxations. However, it has been used very rarely in studies of alloy surfaces[31] and to our knowledge no measurements of surface segregation effects have been reported. A full account of the MEIS-SB method is given in Ref. 32.

In this study, we use MEIS-SB to determine the atomic composition in the first three layers of the $Pt_{0.5}Ni_{0.5}(111)$ surface. In principle, many parameters could be determined in this experiment: the Pt and Ni concentrations of the first, second and third crystal layers (denoted respectively as C_1^{Pt}, C_1^{Ni}, C_2^{Pt}, C_2^{Ni}, C_3^{Pt}, and C_3^{Ni}), the values of the first and second interlayer distances (D_{12} and D_{23}) and the thermal vibration amplitudes of the atoms in the first, second, and third layers (U_1, U_2, and U_3). Since the platinum and nickel data were treated separately, both nickel and platinum concentrations are used throughout this work.

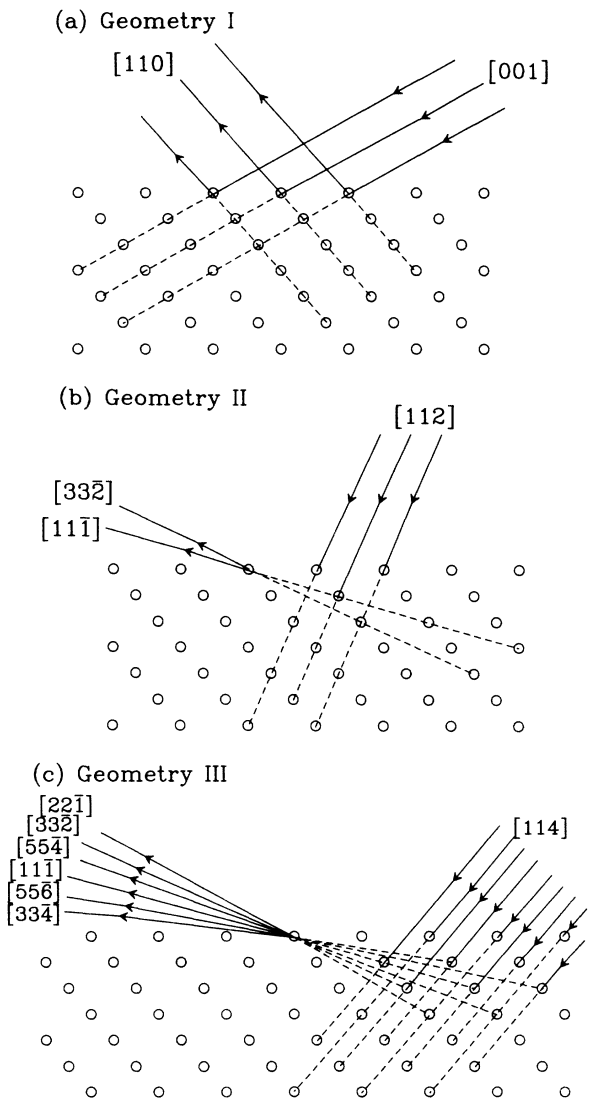

FIG. 1. Three different scattering geometries (I, II, and III), all in the ($\bar{1}$10) plane perpendicular to the $Pt_{0.5}Ni_{0.5}(111)$ surface. (a) In geometry I, the beam is aligned with the [001] rows which terminate in the first atomic layer. (b) In geometry II, the beam is aligned with the [112] rows which terminate in the first and second atomic layer. (c) In geometry III, the beam is aligned with the [114] rows which terminate in the first three layers.

In order to uniquely determine all variables, measurements were made in three different backscattering geometries (Fig. 1). The blocking patterns taken in these geometries were compared, by means of a χ^2 analysis, with Monte Carlo computer simulations of the backscattering experiment for a range of different concentrations, relaxations and vibration amplitudes. A search was made for the best fit to the data.

The paper is organized as follows. In Sec. II the details of sample preparation and the MEIS-SB technique are explained. In Sec. III the results are presented by showing typical backscattering energy spectra and blocking patterns of the platinum and nickel yields for the three different scattering geometries. Section IV describes the Monte Carlo simulations and the search for the best composition model, including relaxations and thermal vibration amplitudes. In Sec. V the results from this analysis are compared with data from LEED *I-V* measurements and with theoretical predictions. Conclusions and summary are given in Sec. VI.

II. EXPERIMENT

The experiments were performed in a UHV system (base pressure of 5×10^{-11} Torr), consisting of a main scattering chamber equipped with LEED and Auger facilities, a preparation chamber with an ion gun for sputter cleaning and a load lock for introducing samples into the vacuum system. A detailed description of the system is given elsewhere.[33,34] Below the sample preparation and the experimental method are briefly described.

A. Crystal preparation

The $Pt_{0.5}Ni_{0.5}$ sample is the same as that studied in Refs. 4 and 11. X-ray analysis[8] evidenced a random substitutional alloy having a fcc lattice with a lattice constant of 3.749 Å, which is close to the tabulated values for a 50% Pt–50% Ni composition (see, e.g., Refs. 35 and 36). The surface was x-ray oriented and mechanically repolished down to a surface roughness of 0.05 μm. It was checked that the misalignment of the surface orientation with respect to the [111] direction was less than 0.2°. The sample was mounted with Ta wires on a Ta holder which could be heated from the rear side with a filament biased at a potential of -500 V with respect to the sample. The assembly was introduced into the preparation chamber and the sample was annealed for several hours at 1200 °C, in order to remove defects introduced by the mechanical polishing. The sample was cleaned by cycles of Ar sputtering (500 eV, 2 μA, 15 min) and annealing up to 1000 °C for 10 min. During the first few cleaning cycles, a graphite overlayer was seen. After several more cycles and by lowering the annealing temperature (last anneal at 600 °C for 4 min) no carbon was detected (detec-

tion limit is less than 2% of a monolayer) while the LEED diagram showed a sharp (1×1) pattern.

B. Ion scattering

After the cleaning procedure, the sample with heating assembly was transferred from the preparation chamber into the scattering chamber and mounted in a high precision goniometer providing three independent rotations and two translations. A beam of 100-keV H^+ ions entered the scattering chamber through a differentially pumped beam line and a set of collimating diaphragms, and was aligned with an axis of the crystal. Ions, backscattered in an angular region of 20° in the $(\bar{1}10)$ scattering plane were energy selected by a toroidal electrostatic analyzer and detected on position sensitive channel plates (the angular resolution is 0.3°, the precision of positioning the detector is 0.05° and the energy resolution, $\Delta E/E$, is 0.4%). A set of 64 angular spectra covering 20° was measured simultaneously. During data acquisition, care was taken not to damage the crystal by moving to a new beam spot after each 200 $\mu C/cm^2$ of beam dose. Measurable damage occurred after a beam dose of 400 $\mu C/cm^2$, as seen by a 5% increase in the platinum surface peak content and an increase of the minimum yield below the nickel peak.

Data analysis involves the extraction of the platinum and nickel surface peak areas from the energy spectra at the different exit angles. With the use of standard calibration procedures[33,37] the surface peak areas were converted into the number of visible monolayers of platinum and nickel. In this way, angular distributions of the number of visible atoms ("blocking patterns") were obtained for the three different scattering geometries, labeled I, II, and III in Fig. 1. In geometry I, the beam is incident along the [001] atom rows and a surface peak area of one visible atom per [001] row is equivalent to one visible monolayer or 1.6×10^{15} atom/cm^2 (which is the atomic density in a single $Pt_{0.5}Ni_{0.5}(111)$ layer). In the two other scattering geometries, II and III in Figs. 1(b) and 1(c), the beam is incident along the [112] and [114] rows which terminate in the first two and the first three atomic planes, respectively. Hence, a yield of one visible atom per [112] row is equivalent to two monolayers or 3.22×10^{15} atom/cm^2 and one visible atom per [114] row equals three monolayers or 4.83×10^{15} atom/cm^2. The geometries II and III provide sensitivity to the determination of platinum and nickel concentrations in the second and third layers, respectively.

III. RESULTS

The energy spectra reveal a strong segregation effect. Typical spectra are shown in Fig. 2. Both spectra were taken in double alignment, in geometry I along the [110] exit angle and in geometry II along the $[33\bar{2}]$ direction. The exit angles are measured with respect to the surface plane. To allow for a direct comparison of the Pt and Ni surface peak intensities, the Ni peaks in Fig. 2 have been multiplied by the ratio of the Pt to Ni Rutherford cross section ($\times7.8$). The Pt peak in the spectrum taken in geometry I is much larger than the scaled Ni peak, which indicates a strong enrichment of platinum in the outermost layer. The second layer, however, must be enriched in nickel, because in geometry II a dramatic increase in the Ni peak intensity is observed. (For clarity, the spectrum for geometry II has been scaled to an equal Pt peak area as the spectrum taken in geometry I.) Thus we are led to a segregation model in which the first layer is strongly enriched in platinum and the second layer is depleted in platinum.

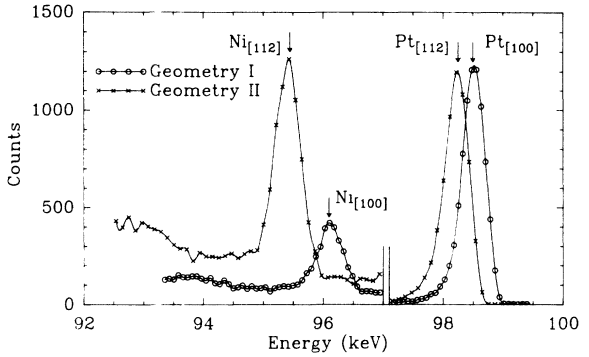

FIG. 2. Two energy spectra measured in geometry I (○) along the [110] direction (54.7° exit angle) and in geometry II (×) along the $[33\bar{2}]$ direction [29.5° exit angle, shown in Figs. 1(a) and 1(b), respectively]. The Ni peaks are multiplied by a factor of 7.8 to correct for the difference in scattering cross section between Pt and Ni. Both spectra are scaled to equal Pt peak contents. The energy shift between the two spectra is caused by a difference in scattering angle. Spectrum II is measured with a larger scattering angle and therefore the Pt and Ni peaks appear at lower energies.

The measured blocking patterns confirm the oscillating segregation model. Geometry I (Fig. 3) shows a flat Pt pattern which mainly originates from the Pt-enriched

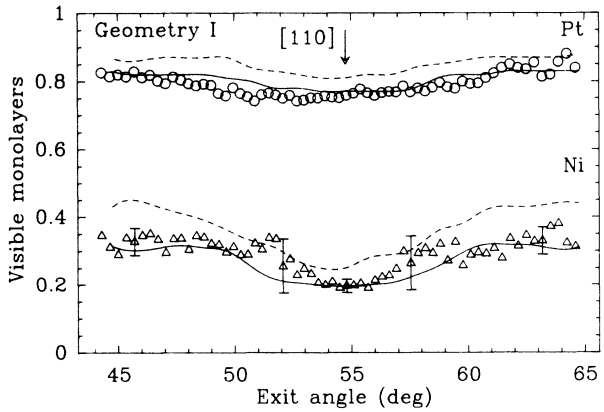

FIG. 3. Number of visible monolayers of Pt (○) and Ni (△) atoms vs exit angle, measured in geometry I. The solid lines represent best-fit computer simulations for the compositional and structural parameters listed in Table I. The dashed curve in the Pt data represents a simulation for a 5%-higher first-layer Pt concentration, while the dashed curve in the Ni data represents a simulation for a 10%-larger thermal vibration amplitude of the first layer. These curves serve to illustrate the sensitivity to variation of the parameters in Table I. The arrow indicates the direction of the bulk axis as defined in Fig. 1.

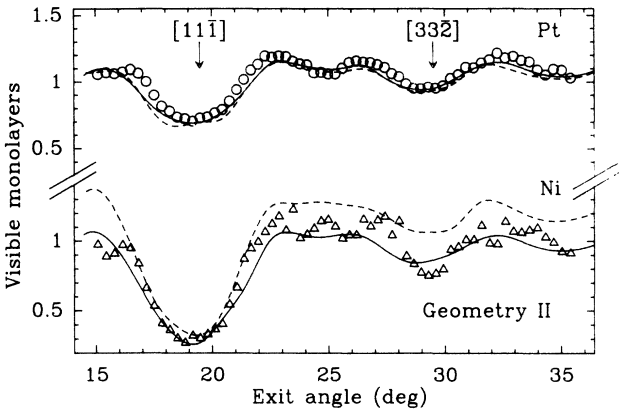

FIG. 4. Blocking patterns, as in Fig. 3, measured in geometry II. The dashed curve in the Pt data represents a simulation for a 20%-lower thermal vibration amplitude of the second layer, while the dashed curve in the Ni data represents a simulation for a 10%-larger second-layer Ni concentration.

outermost layer, and a single broad minimum in the much lower Ni yield. This lower yield evidences a small nickel concentration in the first layer. The pronounced Ni blocking minimum and the lack of a corresponding minimum in the platinum yield reflect the large concentration of second-layer Ni atoms. Since in this configuration only a small amount of nickel is seen, the relative contribution of the background becomes of importance, especially between 2° and 4° beside the [110] direction, where dechanneling and focusing phenomena play a role. This is reflected in the large errors in the nickel blocking pattern, not only in this geometry but also around the [33$\bar{2}$] direction in geometry II and around several minima in geometry III. Due to the larger scattering cross section, no background subtraction problems occurred with the platinum data.

In geometry II (Fig. 4), the second layer contributes as much as the first layer; the Ni yield is much increased and exhibits a pronounced blocking minimum, while shallow blocking minima are also observed in the Pt

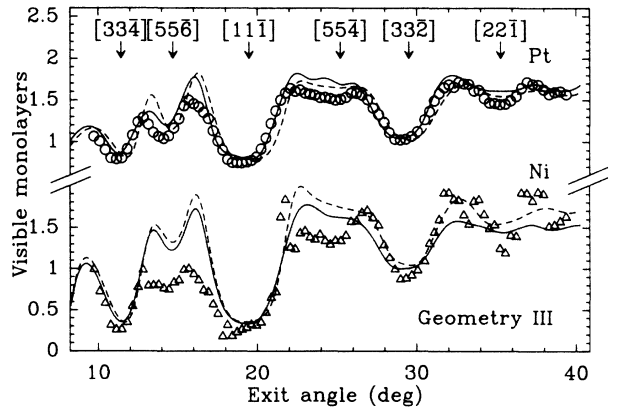

FIG. 5. Blocking patterns, as in Fig. 3, measured in geometry III. The dashed curve in the Pt data represents a simulation with no relaxations in the first and second layers while the dashed curve in the Ni data represents a simulation for a 10%-larger third-layer Ni concentration.

yield. For exit angles outside the blocking minima, both the Pt and the Ni yields are equal to ~1 monolayer, precisely as expected for an average composition of 50%–50%. Thus the percentage of Pt *enrichment* in the first layer is roughly equal to the percentage of platinum *depletion* in the second layer.

Finally, in geometry III (Fig. 5), a multitude of blocking minima is observed, whereas the Pt and Ni yields both equal ~1.5 monolayer in single alignment. The ~0.5 monolayer increase in the Pt and Ni yield with respect to the yields in geometry II represent the contribution of the third layer which apparently has a composition close to 50%-50%. We conclude that the oscillation in the platinum and nickel concentrations is essentially damped out over a depth of three atomic layers.

IV. SEGREGATION PROFILE

The concentrations of Pt and Ni in the first three atomic layers are quantitatively determined by performing Monte Carlo simulations of the experiment for different segregation profiles and fitting those to the measured blocking patterns. The simulation method used is that developed by Frenken *et al.*,[38] but modified to account for the scattering from two different, randomly distributed, atom types in the crystal. It is assumed that the crystal has bulk properties beneath the third layer and that the thermal vibration amplitudes of Pt and Ni atoms are equal at room temperature, even in the surface layers, where the vibration amplitudes are enhanced (with Debye temperatures of 225 °C for Pt and 425 °C for Ni a bulk one-dimensional root-mean-square thermal vibration amplitude of 0.066 Å is calculated for both the pure metals).

Theoretical investigations evidence an anisotropy in the thermal vibration amplitudes of surface-layer atoms.[39,40] Therefore, the thermal vibration amplitudes were allowed to be anisotropic, with the component perpendicular to the surface three times as large as the lateral vibration amplitudes. Also, correlated thermal vibrations and connections of ingoing and outgoing trajectories have been considered, but these three effects were not taken into account in the final calculations, since the blocking patterns and the best-fit structure parameters appeared only very little affected by these modifications.[38]

For a particular set of parameters, blocking patterns were simulated for both elements and for all three geometries. The resulting six blocking patterns were compared with the data using a reduced χ^2 goodness-of-fit criterion. A search was made for a *combined* minimum in χ^2 for *all* six blocking patterns. All parameters were allowed to vary simultaneously within the range denoted in the first column of Table I. Due to the three different geometries, the correlations between most parameters are very small, so that in the final calculations only four parameters were allowed to vary simultaneously.

The resulting optimal values for the parameters are listed in Table I. The errors are calculated from the combined χ^2 values. Due to different scattering cross sections, the uncertainties in the nickel data are larger than

TABLE I. The results of a search for the best fit between simulated and measured blocking patterns. The parameters used in the calculations are the Pt and Ni concentrations for the first three layers, C_i^{Pt} and C_i^{Ni}, the enhancement of the thermal vibration amplitudes of the first three layers, U_i, with respect to the bulk values U_b of 0.066 Å, and the changes ΔD_{12} and ΔD_{23} in the first two interlayer spacings with respect to the bulk interlayer spacing of 2.164 Å. This one set of values yielded the best fit to all experimental blocking patterns simultaneously.

Parameter	Range (%)	Concentration (%)
C_1^{Pt}	40–90	75±3
C_1^{Ni}	10–60	16±5
C_2^{Pt}	10–50	27±4
C_2^{Ni}	50–90	71±5
C_3^{Pt}	30–75	53±6
C_3^{Ni}	30–75	46±6
U_1/U_b	100–200	148±10
U_2/U_b	100–150	121±10
U_3/U_b	100–120	108±10
$\Delta D_{12}/D_b$	−6 to 0	−2.0±1.0
$\Delta D_{23}/D_b$	−6 to 0	−2.0±1.0

the platinum errors, as is reflected in the quality of the fits to the nickel data. This difference is taken into account in the χ^2 search.

The main result from these simulations is an accurate determination of the composition profile. Furthermore, the damped oscillation of the platinum concentration is accompanied by a small inward relaxation of the first and second interlayer distances. The thermal vibration amplitudes of the first two layers show a significant increase, leading to a vibration amplitude for the first-layer atoms of almost one and half times the bulk value.

MEIS-SB is quite sensitive to changes in any of the parameters listed in Table I. This is illustrated by the dashed blocking patterns of Figs. 3, 4, and 5 which represent calculations in which only a single parameter is changed and the other parameters are kept fixed at the optimum values.

Figure 6 demonstrates the high sensitivity of the measurements in geometry I, II, and III to the platinum and nickel concentrations in the first, second, and third layers, respectively. In this figure, χ^2 values are plotted which measure the goodness of fit between experimental and calculated blocking patterns for a large range of different concentrations. For each curve in Fig. 6 only one concentration is changed, with the other parameters fixed at their best-fit values. Since the analysis was done separately for the two elements and the three scattering geometries, six different sets of χ^2 values are shown.

The minima for the six sets of χ^2 values correspond with the concentrations presented in Table I. It is seen that the fits to the Pt data have a lower minimum in χ^2 than the Ni fits. This shows that with our model the goodness of fit to the Pt data is somewhat better than the fit to the Ni data. Furthermore, the minimum in χ^2 becomes more shallow for deeper layers. This causes the larger error bars for C_3^{Pt} and C_3^{Ni} in Table I.

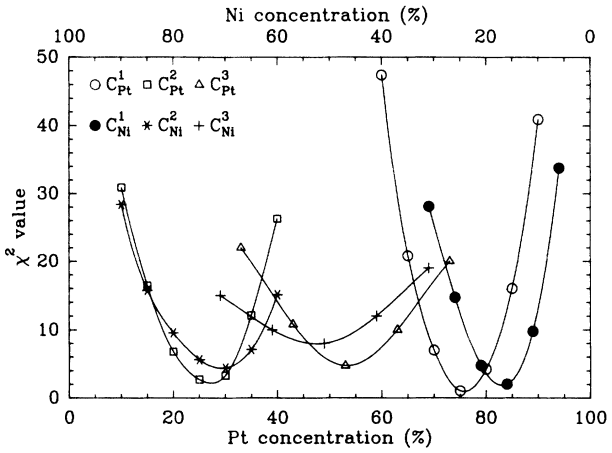

FIG. 6. χ^2 goodness-of-fit values resulting from a comparison of the experimental Pt and Ni blocking patterns with calculated blocking patterns for different concentrations of Pt and Ni. The curves marked by symbols (○) and (●) display the goodness of fit between the blocking patterns measured in geometry I from Pt and Ni, and the corresponding patterns calculated for a range of different concentrations C_1^{Pt} and C_1^{Ni}, respectively. Likewise, the curves marked as (□) and (*) show the goodness of fit between Pt and Ni blocking patterns taken in geometry II and the corresponding patterns calculated for different C_2^{Pt} and C_2^{Ni} values. Finally, the curves (△) and (+) display the goodness of fit between the blocking patterns taken in geometry III and the patterns calculated for different concentrations C_3^{Pt} and C_3^{Ni}.

V. DISCUSSION

The most remarkable result of this study is the platinum enrichment on the surface, although nickel has the lowest sublimation energy,[41] a well-known criterion to predict which element will segregate. The inward relaxation of the first two atom layers is found on many clean metal surfaces.[32] The enhancements of the thermal vibration amplitudes are predicted theoretically by Clark[39] and Masuda.[40] Our values are in close agreement with their predictions and with other MEIS-SB experiments. However, the thermal vibration amplitudes are average values. The enhancements might partly be due to static displacements of atoms. Yalisove *et al.*[31] have observed a pronounced "buckling" effect on a Ni-Al alloy surface. However, the positions of the platinum and nickel blocking minima in the second and third geometries do not differ much. Therefore we conclude that this "buckling" effect plays a minor role in the Pt-Ni system.

The concentrations and relaxations of the first three layers of the $Pt_{0.5}Ni_{0.5}(111)$ surface have also been determined by other methods and predicted theoretically (see the Introduction). The results of the different experimental techniques are shown, together with theoretical predictions of the embedded-atom method and the tight-binding Ising model, in Table II.

Both the EAM and the TBIM methods (shown in the fourth and fifth columns of Table II, respectively) give results which are close to the MEIS-SB data presented in this paper (given in the last column of the same table). The LEED *I-V* (first column) and MEIS-SB results are in

TABLE II. A comparison of our best-fit values for the Pt concentrations in the first three atomic layers and the relaxations of the first two interlayer distances with the values obtained from other experimental work [LEED *I-V* (Ref. 11), IDEAS (Ref. 15) and LEIS (Ref. 17)] and from theoretical calculations [EAM (Ref. 23) and TBIM (Refs. 24 and 25)]. All values are expressed in %.

	LEED *I-V*	IDEAS	LEIS	EAM	TBIM	Present work
C_1^{Pt}	88±2	95±10	88±4	68	70	75±2
C_2^{Pt}	9±5	0±20		31	43	27±3
C_3^{Pt}	65±10			56	52	54±5
$\Delta D_{12}/D_b$	−1.0±			−5.3		−2.0±0.5
$\Delta D_{23}/D_b$	−2.4±			−1.4		−2.0±0.5

qualitative agreement. The oscillatory behavior is found in both cases and also the inward relaxations are equal within the experimental errors. The oscillating segregation effect is more pronounced in the LEED *I-V* data.

The incidence-dependent Auger measurements (IDEAS) (Ref. 15) (second column) are in agreement with the LEED *I-V* results and not with our ion scattering data, but the uncertainties in the IDEAS work are much larger than those of LEED *I-V* and of MEIS-SB.

Low-energy ion scattering (LEIS) experiments (third column) confirm the LEED *I-V* data for the first-layer concentrations.[16–18] They also observe an influence of the annealing temperature on the first-layer concentrations. However, since in these LEIS measurements no time-of-flight detection was employed, high ion-beam doses had to be used, giving rise to considerable sputtering effects and, possibly, to different concentrations.

A possible explanation for the discrepancy between the LEED *I-V* data and our results is the different preparation of the crystal. In the LEED experiments the sample was annealed up to 1000 °C, where in this study only 600 °C was used, in order to avoid carbon contamination. Apart from a possible carbon contamination after the 1000 °C anneal, the thermodynamical equilibrium concentrations could be different. Evidence for this is given by high-temperature LEIS measurements by Temmerman.[17]

VI. CONCLUSIONS

Medium-energy ion scattering combined with shadowing and blocking is well suited for studying depth-dependent surface segregation effects in binary alloys, provided there is a reasonable mass difference between the two components (like most platinum-based alloys). On the $Pt_{0.5}Ni_{0.5}(111)$ surface an oscillating segregation is found, with (75±2)% Pt in the first layer, (27±2)% Pt in the second layer, and (53±5)% Pt in the third layer. An inward relaxation is found for the first two interlayer distances of (−2.0±0.5)% and (−2.0±0.5)% with respect to the bulk values. The enhancements of the thermal vibration amplitudes of the first three layers are found to be 148, 128 and 108% with respect to the bulk values, respectively. The measurements are in excellent agreement with embedded-atom and tight-binding Ising types of calculations, and are also in qualitative agreement with LEED *I-V* studies of this surface. In our measurements a less pronounced segregation effect is seen than in the LEED *I-V* analysis. In particular, a much larger Pt concentration in the second layer is found.

ACKNOWLEDGMENTS

The authors would like to thank Dr. J. W. M. Frenken for assistance with adapting the Monte Carlo computer code for simulations on alloys, and J. Kuiper for polishing the Pt-Ni sample. Professor Dr. J. W. Geus, Dr. Y. Gauthier, Professor Dr. J. C. Bertolini, Dr. H. Vrijmoeth and Dr. H. W. Slijkerman are thanked for many helpful discussions. This work is done within the framework of the European Science Foundation Network for Surface Crystallography and is part of the research program of the Stichting Scheikundig Onderzoek Nederland. It is made possible by financial support from the Nederlandse Organisatie voor Wetenschappelijk Onderzoek (the Netherlands Organization for Scientific Research.)

[1] A. Wielers, G. Zwolsman, C. van der Grift, and J. Geus, Appl. Catal. **19**, 187 (1985).

[2] A. Renouprez, B. Moraweck, M. Dominiquez, V. Prichon, and B. Imelik, C. R. Acad. Sci. **C286**, 303 (1978).

[3] J. Sedláçek, L. Hilaire, P. Légaré, and G. Maire, Appl. Surf. Sci. **10**, 75 (1982).

[4] J. Massardier and J. Bertolini, J. Catal. **90**, 358 (1984).

[5] Y. Jugnet, J. Bertolini, J. Massardier, B. Tardy, T. Minh Duc, and J. Vedrine, Surf. Sci. **107**, L320 (1981).

[6] J. Bertolini, J. Massardier, and B. Tardy, J. Chim. Phys. **78**, 939 (1981).

[7] J. Bertolini, B. Tardy, M. Abon, J. Billy, P. Delichère, and J. Massardier, Surf. Sci. **135**, 117 (1983).

[8] Y. Gauthier, R. Baudoing, Y. Joly, J. Rundgren, J. Bertolini, and J. Massardier, Surf. Sci. **162**, 324 (1985).

[9] Y. Gauthier, Y. Joly, R. Baudoing, and J. Rundgren, Phys. Rev. B **31**, 6216 (1985).

[10] R. Baudoing, Y. Gauthier, M. Lundberg, and J. Rundgren, J. Phys. C **19**, 2825 (1986).

[11] Y. Gauthier, R. Baudoing, M. Lundberg, and J. Rundgren, Phys. Rev. B **35**, 7867 (1987).

[12] Y. Gauthier, R. Baudoing, and J. Jupille, Phys. Rev. B **40**,

1500 (1989).
[13]J. Bertolini, J. Massardier, P. Delichère, B. Tardy, B. Imelik, Y. Jugnet, and T. Minh Duc, Surf. Sci. **119**, 95 (1982).
[14]Y. Jugnet, N. Prakash, G. Grenet, T. Minh Duc, and H. Poon, Surf. Sci. **189-190**, 649 (1987).
[15]J. Segaud, E. Blanc, C. Lauroz, and R. Baudoing, Surf. Sci. **206**, 297 (1989).
[16]L. de Temmerman *et al.*, Le Vide, les Couches Minces **217**, 275 (1983).
[17]L. de Temmerman, C. Creemers, H. van Hove, A. Neyens, J. Bertolini, and J. Massardier, Surf. Sci. **178**, 888 (1986).
[18]L. de Temmerman, C. Creemers, H. van Hove, and A. Neyers, Surf. Sci. **183**, 565 (1987).
[19]F. Williams and D. Nason, Surf. Sci. **45**, 377 (1974).
[20]F. Abraham, N.-H. Tsai, and G. Pound, Surf. Sci. **83**, 406 (1979).
[21]J. Chelikowsky, Surf. Sci. **139**, L197 (1984).
[22]S. Mukherjee and J. Morán-López, Surf. Sci. **189-190**, 1135 (1987).
[23]M. Lundberg, Phys. Rev. B **36**, 4692 (1987).
[24]B. Legrand and G. Tréglia, in *The Structure of Surfaces II*, edited by J. van der Veen and M. Van Hove (Springer-Verlag, Heidelberg, 1988), Vol. 2, p. 167.
[25]G. Tréglia and B. Legrand, Phys. Rev. B **35**, 4338 (1987).
[26]R. Donelly and T. King, Surf. Sci. **74**, 89 (1978).
[27]T. King and R. Donnelly, Surf. Sci. **141**, 417 (1984).
[28]P. Arroyo and J. Joud, J. Phys. (Paris) **48**, 1721 (1987).
[29]P. Arroyo and J. Joud, J. Phys. (Paris) **48**, 1733 (1987).
[30]J. Eymery and J. Joud, Lab. de Thermodynamique et Physico-Chemie Métallurgiques (Université Joseph Fourier, Grenoble), technical report, 1988 (unpublished).
[31]S. Yalisove and W. Graham, J. Vac. Sci. Technol. A **6**, 588 (1988).
[32]J. van der Veen, Surf. Sci. Rep. **5**, 199 (1985).
[33]W. Turkenburg, W. Soshka, F. Saris, H. Kersten, and B. Colenbrander, Nucl. Instrum. Methods **132**, 587 (1976).
[34]R. Smeenk, R. Tromp, H. Kersten, A. Boerboom, and F. Saris, Nucl. Instrum. and Methods **195**, 581 (1982).
[35]R. Hultgren, P. Desai, D. Hawkins, M. Gleiser, and K. Kelley, *Thermodynamic Properties of Binary Alloys* (American Society for Metals, Metals Park, OH, 1973).
[36]D. Hanson, J. Inst. Met. **55**, 117 (1934).
[37]J. Frenken, R. Tromp, and J. van der Veen, Surf. Sci. **172**, 319 (1986).
[38]J. Frenken, R. Tromp, and J. van der Veen, Nucl. Instrum. and Methods B **17**, 334 (1986).
[39]B. Clark, R. Herman, and R. Wallis, Phys. Rev. **139**, A860 (1965).
[40]K. Masuda, Phys. Rev. B **26**, 5968 (1982).
[41]C. Kittel, *Introduction to Solid State Physics*, 6th ed. (Wiley, New York, 1986).